

Article

Thermodynamic Modeling of the Au-Ge-X (X = In, Sb, Si, Zn) Ternary Systems

Yuchen Bai, Qingsong Tong, Maohua Rong *, Cong Tan, Xingyu Liu, Man Li and Jiang Wang *

School of Materials Science and Engineering & Guangxi Key Laboratory of Information Materials, Guilin University of Electronic Technology, Guilin 541004, China; 13124132992@163.com (Y.B.); 13635644432@163.com (Q.T.); tancong0526@163.com (C.T.); liuxingyu0026@163.com (X.L.); liman560209@163.com (M.L.)

* Correspondence: rongmh124@guet.edu.cn (M.R.); waj124@guet.edu.cn (J.W.)

Abstract: In this study, the CALPHAD approach was employed to model the thermodynamics of the Au-Ge-X (X = In, Sb, Si, Zn) ternary systems, leveraging experimental phase equilibria data and previous assessments of related binary subsystems. The solution phases were modeled as substitutional solutions, and their excess Gibbs energies were expressed using the Redlich–Kister polynomial. Owing to the unavailability of experimental data, the solubility of the third elements in the Au-In, Au-Sb, and Au-Zn binary intermetallic compounds was excluded from consideration. Additionally, stable ternary intermetallic compounds were not reported in the literature and, thus, were not taken into account in the present thermodynamic calculations. Calculations of liquidus projections, isothermal sections, and vertical sections for these ternary systems have been performed, aligning with existing experimental findings. These thermodynamic parameters form a vital basis for creating a comprehensive thermodynamic database for Au-Ge-based alloys, which is essential for the design and development of new high-temperature Pb-free solders.

Keywords: Au-Ge based alloys; phase equilibria; thermodynamics; CALPHAD



Citation: Bai, Y.; Tong, Q.; Rong, M.; Tan, C.; Liu, X.; Li, M.; Wang, J. Thermodynamic Modeling of the Au-Ge-X (X = In, Sb, Si, Zn) Ternary Systems. *Materials* **2024**, *17*, 2137. <https://doi.org/10.3390/ma17092137>

Academic Editor: Frank Czerwinski

Received: 24 March 2024

Revised: 26 April 2024

Accepted: 30 April 2024

Published: 2 May 2024



Copyright: © 2024 by the authors. Licensee MDPI, Basel, Switzerland. This article is an open access article distributed under the terms and conditions of the Creative Commons Attribution (CC BY) license (<https://creativecommons.org/licenses/by/4.0/>).

1. Introduction

The Pb-5wt. % Sn solder is commonly employed as a high-temperature solder in electronic packaging within the modern electronics industry. The environmental and health risks associated with lead necessitate research into high-temperature solders devoid of lead, aiming to supplant conventional solders that have high lead content. [1–3].

Gold-based alloys, such as Au-Sn, Au-Sb, and Au-Ge eutectic alloys, are recognized for their exceptional corrosion resistance, high electrical and mechanical strength, and superior thermal conductivity. These attributes render them highly advantageous for electronic packaging applications [4–8]. Au-Ge-based alloys have especially attracted much attention as high-temperature Pb-free solders [4,9]. To mitigate the costs of Au-based alloys, alloying elements, such as Ag, Bi, Cu, Ga, Ge, In, Sb and Zn, can be introduced to partially replace Au. In order to comprehensively understand the impact of alloying elements, a thorough understanding of the reliable phase equilibria and thermodynamic properties of Au-based alloys is essential. This knowledge is critical for the development of advanced high-temperature Pb-free solders based on Au, contributing to significant advancements in electronic packaging materials.

The literature [10–20] contains reports on thermodynamic calculations for various Au-based alloy systems, including Au-Ag-Si, Au-Ag-Pb, Au-Ge-Ni, Au-Si-Sn, Au-Bi-Sb, Au-Ge-Cu, Au-Ge-Sn, Au-Ag-Sn, Au-In-Sn, Au-Sb-Si, and Au-Ge-Sb. Despite this extensive coverage, there appears to be a lack of reported data on the thermodynamic calculations for the Au-Ge-In, Au-Ge-Si, and Au-Ge-Zn ternary systems. Although the thermodynamic model of the Au-Ge-Sb system by Wang et al. [15] aligns well with experimental outcomes,

recent updates have been made to the thermodynamic parameters of its binary subsystems [21]. Consequently, there is an ongoing need to re-optimize the Au-Ge-Sb ternary system. Therefore, the objective of this study was to conduct thermodynamic calculations of phase equilibria in the Au-Ge-X (X = In, Sb, Si, Zn) ternary systems using the CALPHAD method. This research serves as a fundamental step toward establishing a comprehensive thermodynamic database for multicomponent Au-based alloy systems.

2. Literature Information

2.1. The Au-Ge-In Ternary System

The literature by Okamoto et al. [22] and Chevalier [23] provides comprehensive reviews of the Au-Ge system. Subsequently, it was re-optimized by Wang et al. [14] using the lattice stability parameters updated by Dinsdale [24]. The optimization outcomes of the Au-Ge system [14] are in accordance with the experimental findings, encompassing phase diagrams and thermodynamic properties. A thermodynamic assessment of the Au-In system was performed by Ansara and Nabot [25]. Liu et al. [26] re-optimized it, taking into account the temperature dependence of the measured enthalpy of mixing of the liquid phase. The Ge-In system was assessed thermodynamically by Chevalier et al. [27]. The calculated results of the Au-In and Ge-In systems [26,27] demonstrate good agreement with the experimental findings. The thermodynamic parameters of the Au-Ge, Au-In, and Ge-In systems obtained by Wang et al. [14], Liu et al. [26], and Chevalier et al. [27] were directly employed in the current calculation of the Au-Ge-In ternary system.

The Au-Ge-In system was studied experimentally by Butt [28], while the thermodynamic properties of this ternary system were not reported in the literature. The experimental results [28] show that two E-type invariant reactions (liquid \leftrightarrow diamond(Ge) + AuIn + AuIn₂ at 744 K, liquid \leftrightarrow diamond(Ge) + AuIn₂ + tetragonal(In) at 429 K) were determined, and four vertical sections of AuIn-Ge, Au_{41.5}In_{58.5}-Ge, AuIn₂-Ge, and Au₂₀In₈₀-Ge were measured. The stable ternary intermetallic compounds in this ternary system were not observed by Butt [28]. The experimental results [28] were taken into account in the present calculation.

2.2. The Au-Ge-Sb Ternary System

The Au-Sb system, a pivotal component of the Au-Ge-Sb system, has been extensively investigated by numerous researchers [19,29–32]. Liu et al. [31] conducted an optimization of the Au-Sb system, taking into account the existing experimental data. The phase diagram and thermodynamic data previously published align well with the recent calculations [30]. The optimization of the Ge-Sb system was initially conducted by Wang et al. [15] and Chevalier et al. [27]. Due to the oversight regarding the solubility of Ge in the rhombohedral Sb phase in these earlier studies, Liu et al. [21] conducted a re-optimization of the Ge-Sb system. The re-optimized results [21] correlate closely with the experimental observations. Consequently, the refined thermodynamic data for the Ge-Sb system from Liu et al. [21], along with the Au-Sb system data from Liu et al. [31], have been incorporated into the current calculations for the Au-Ge-Sb system.

Zwingmann [33] conducted a study on the phase equilibria of the Au-Ge-Sb system; however, the thermodynamic properties of this system have not been reported in the literature. Prince et al. [34] conducted a review of the Au-Ge-Sb system as part of their compilation of Au-based alloy phase diagrams. According to the experimental results [33], the Au-Ge-Sb system contains two invariant reactions: the peritectic reaction (U), liquid + rhombohedral (Sb) \leftrightarrow diamond (Ge) + AuSb₂ at 703 K and the eutectic reaction (E), liquid \leftrightarrow diamond (Ge) + fcc (Au) + AuSb₂ at 561 K. Three vertical sections of AuSb₂-Ge, Ge_{0.1}Sb_{0.9}-Au, and 15 at.% Ge were measured by Zwingmann [33]. Zwingmann [33] did not observe the presence of stable ternary intermetallic compounds in the Au-Ge-Sb system.

The Au-Ge-Sb system was optimized by Wang et al. [15]. Afterward, Liu et al. [21] updated the thermodynamic parameters of the Ge-Sb system. Liu et al. [21] took into account the solubility of Ge in rhombohedral(Sb) during the optimization of the Ge-Sb system. The

thermodynamic assessment of the Au-Ge-Sb system by Wang et al. [15] was found to be in good agreement with the experimental data [33]. However, updated thermodynamic parameters for the Ge-Sb systems were provided by Liu et al. [21], indicating a necessity to re-optimize the Au-Ge-Sb system based on the findings reported in reference [33].

2.3. The Au-Ge-Si Ternary System

Meng et al. [20] conducted optimization studies on the Au-Si system, while Olesinski and Abbaschian [35] and Bergman et al. [36] focused on reviewing and optimizing the Ge-Si system, respectively. The optimization results for the Au-Si and Ge-Si systems from references [20,36] were well-aligned with the experimental findings and were, therefore, integrated into the current modeling of the Au-Ge-Si system.

While the literature does not detail the thermodynamic properties of the Au-Ge-Si system, Predel et al. [37] have explored its phase equilibria using thermal and metallographic analyses. They identified four vertical sections, namely Au-Ge_{0.20}Si_{0.80}, Au-Ge_{0.40}Si_{0.60}, Au-Ge_{0.60}Si_{0.40}, and Au-Ge_{0.80}Si_{0.75}, and constructed the liquidus projection for this system. The experimental findings from Predel et al. [37] have been incorporated into the ongoing calculations for the Au-Ge-Si system.

2.4. The Au-Ge-Zn Ternary System

The Au-Zn system was assessed by Okamoto and Massalski and Krachler et al. [38,39]. Liu et al. [40] provided an updated thermodynamic assessment of the Au-Zn system. The thermodynamic calculation of the Ge-Zn system was performed by Chewvalier et al. [27]. The calculated results of the Au-Zn and Ge-Zn systems by Liu et al. [40] and Chewvalier et al. [27] are in accordance with experimental data and were consequently utilized in the present calculation of the Au-Ge-Zn system.

As for the phase equilibria of the Au-Ge-Zn system, the vertical section of AuZn-Ge was investigated by Butt et al. [41] using differential thermal analysis (DTA) and the metallographic technique. Their experimental vertical section shows a pseudo-binary eutectic characteristic, and the eutectic composition and temperature were determined to be 12.2 ± 0.2 at.% Ge and 946 K, respectively. At the eutectic temperature, the solubility of Ge in the AuZn alloy was determined to be 1.3 atomic percent Ge, as reported in reference [41]. These experimental findings [41] were utilized in the current calculations.

3. Thermodynamic Models

3.1. Solution Phases

The solution phase ϕ is described by substituting the solution model. It includes liquid, diamond(Ge, Si), tetragonal(In), hcp(Zn), fcc(Au), α (Au, In), hcp(Au, In), rhombohedral(Sb), and ϵ_1 -Au₃Zn₁₇ in the Au-Ge-X (X = In, Sb, Si, Zn) systems. The molar Gibbs energy of the solution phase ϕ is denoted as:

$$G_m^\phi = \sum_{i=\text{Au,Ge,X}} x_i {}^0G_i^\phi + RT \sum_{i=\text{Au,Ge,X}} x_i \ln x_i + {}^E G_m^\phi \quad (1)$$

The mole fraction of each element i(Au, Ge, In, Sb, Si, Zn) is denoted as x_i . The molar Gibbs energy for the phase ϕ of each element, extracted from the SGTE database [24], is represented as ${}^0G_i^\phi$. The constant R represents the gas constant, and T symbolizes the absolute temperature measured in Kelvin. The excess Gibbs energy for phase ${}^E G_m^\phi$ is articulated through the Redlich–Kister–Muggianu polynomial, as documented in reference [42,43]:

$${}^E G_m^\phi = x_{\text{Au}} x_{\text{Ge}} \sum_{j=0}^n (j) L_{\text{Au,Ge}}^\phi (x_{\text{Au}} - x_{\text{Ge}})^j + x_{\text{Au}} x_{\text{X}} \sum_{j=0}^n (j) L_{\text{Au,X}}^\phi (x_{\text{Au}} - x_{\text{X}})^j + x_{\text{Ge}} x_{\text{X}} \sum_{j=0}^n (j) L_{\text{Ge,X}}^\phi (x_{\text{Ge}} - x_{\text{X}})^j + x_{\text{Au}} x_{\text{Ge}} x_{\text{X}} L_{\text{Au,Ge,X}}^\phi \quad (2)$$

$$L_{\text{Au,Ge,X}}^\phi = x_{\text{Au}} ({}^0) L_{\text{Au,Ge,X}} + x_{\text{Ge}} ({}^1) L_{\text{Au,Ge,X}} + x_{\text{X}} ({}^2) L_{\text{Au,Ge,X}} \quad (3)$$

$${}^{(j)}L_{\text{Au,Ge,X}} = A_i + B_i T \quad (4)$$

The binary interaction parameters, ${}^{(j)}L_{\text{Au,Ge}}$, ${}^{(j)}L_{\text{Au,X}}$, and ${}^{(j)}L_{\text{Ge,X}}$ ($X = \text{In, Sb, Si, Zn}$) were taken from the Au-Ge, Au-In, Au-Sb, Au-Si, Au-Zn, Ge-In, Ge-Sb, Ge-Si, and Ge-Zn systems assessed by Wang et al. [14], Liu et al. [26], Liu et al. [31], Meng et al. [20], Liu et al. [40], Chewvalier et al. [27], Liu et al. [21], and Bergman et al. [36], respectively. The ternary interaction parameters, ${}^{(j)}L_{\text{Au,Ge,In}}$, ${}^{(j)}L_{\text{Au,Ge,Sb}}$, ${}^{(j)}L_{\text{Au,Ge,Si}}$, and ${}^{(j)}L_{\text{Au,Ge,Zn}}$ ($j = 0, 1, 2$) are to be assessed in this work.

3.2. Intermetallic Compounds

Nine Au-In intermetallic compounds (α (Au, In), β -Au₄In, β' -Au₄In, γ -Au₉In₄, γ' -Au₇In₃, ψ -Au₃In₂, Au₃In, AuIn, and AuIn₂), one Au-Sb intermetallic compound (AuSb₂), and eleven Au-Zn intermetallic compounds (α_1 -Au₃Zn, α_2 -Au₃Zn, α_3 -Au₃Zn, ϵ_1 -Au₃Zn₁₇, ϵ_2 -Au₃Zn₁₇, β_1 -AuZn, Au₅Zn₃, δ_1 -Au₁₁Zn₁₄, γ_1 -AuZn₃, γ_2 -AuIn₃ and γ_3 -AuZn₃) are stable in the Au-In, Au-Sb, and Au-Zn systems. There are no stable ternary intermetallic compounds in the Au-Ge-X ($X = \text{In, Sb, Si, Zn}$) systems. The crystal structure data of the solid solution phases in the Au-Ge-X ($X = \text{In, Sb, Si, Zn}$) systems are shown in Table 1.

Table 1. Crystallographic data of the solid solution phases in the Au-Ge-X ($X = \text{In, Sb, Si, Zn}$) systems.

Phase	Prototype	Space Group	Pearson Symbol	Thermodynamic Model	Reference
fcc (Au)	Cu	Fm $\bar{3}$ m	cF4	(Au)	[26]
diamond (Ge/Si)	Diamond	Fd $\bar{3}$ m	cF8	(Ge)/(Si)	[35]
tetragonal (In)	In	I4/mmm	tI2	(In)	[26]
rhombohedral (Sb)	As	R $\bar{3}$ m	hR6	(Sb)	[31]
hcp (Zn)	Mg	P6 ₃ /mmc	hP2	(Zn)	[40]
hcp (Au, In)	Mg	P6 ₃ /mmc	hP2	(Au, In)	[26]
α (Au, In)	Ni ₃ Ti	P6 ₃ /mmc	hP16	(Au, In)	[26]
β -Au ₄ In	Cu ₁₁ Sb ₃	Amm2	—	(Au) _{0.785} : (In) _{0.215}	[26]
β' -Au ₄ In	Cu ₁₀ Sb ₃	—	—	(Au) _{0.77778} : (In) _{0.22222}	[26]
γ -Au ₉ In ₄	Cu ₉ Al ₄	P $\bar{4}$ 3m	cP52	(Au) _{0.69231} : (Au, In) _{0.23077} : (In) _{0.07692}	[26]
γ' -Au ₇ In ₃	Au ₇ In ₃	P3	hP60	(Au) _{0.7} : (In) _{0.3}	[26]
ψ -Au ₃ In ₂	Ni ₂ Al ₃	P3m1	hP5	(Au) _{0.5} : (Au, In) _{0.33333} : (In) _{0.16667}	[26]
Au ₃ In	Cu ₃ Ti	Pmmn	oP8	(Au) _{0.75} : (In) _{0.25}	[26]
AuIn	—	—	—	(Au) _{0.5} : (In) _{0.5}	[26]
AuIn ₂	CaF ₂	Fm $\bar{3}$ m	cF12	(Au) _{0.33333} : (In) _{0.66667}	[26]
AuSb ₂	FeS ₂	Pa3	cP12	(Au) _{0.33333} : (Sb) _{0.66667}	[31]
α_1 -Au ₃ Zn	Ag ₃ Mg	—	—	(Au) _{0.6} : (Au, Zn) _{0.2} : (Zn) _{0.2}	[40]
α_2 -Au ₃ Zn	—	Abam (Cmca)	oC32	(Au) _{0.75} : (Zn) _{0.25}	[40]
α_3 -Au ₃ Zn	Cu ₃ Pd	Pn2n/Pnmm	—	(Au) _{0.64286} : (Au, Zn) _{0.25} : (Zn) _{0.10714}	[40]
ϵ_1 -Au ₃ Zn ₁₇	Mg	P6 ₃ /mmc	hP2	(Au, Zn)	[40]
ϵ_2 -Au ₃ Zn ₁₇	—	—	—	(Au) _{0.15} : (In) _{0.85}	[40]
β_1 -AuZn	CsCl	Pm $\bar{3}$ m	cP2	(Au, Zn) _{0.5} : (Au, Zn) _{0.5}	[40]

Table 1. Cont.

Phase	Prototype	Space Group	Pearson Symbol	Thermodynamic Model	Reference
Au ₅ Zn ₃	—	Ibam	—	(Au) _{0.625} : (Zn) _{0.375}	[40]
δ ₁ -Au ₁₁ Zn ₁₄	—	—	—	(Au) _{0.44} : (Zn) _{0.56}	[40]
γ ₁ -AuZn ₃	Cu ₅ Zn ₈	—	—	(Au, Zn) _{0.15385} : (Au) _{0.15385} : (Au, Zn) _{0.23077} : (Zn) _{0.46153}	[40]
γ ₂ -AuZn ₃	H ₃ U	Pn $\bar{3}$ m	cP32	(Au) _{0.25} : (Zn) _{0.75}	[40]
γ ₃ -AuZn ₃	—	—	—	(Au) _{0.12} : (Au, Zn) _{0.16} : (Zn) _{0.72}	[40]

Based on the calculated results of the Au-In, Au-Sb, and Au-Zn systems by Liu et al. [26], Wang et al. [31], and Liu et al. [40], the molar Gibbs energies of these intermetallic compounds (β -Au₄In, β' -Au₄In, γ' -Au₇In₃, Au₃In, AuIn, AuIn₂, AuSb₂, α_2 -Au₃Zn, ϵ_2 -Au₃Zn₁₇, β_1 -AuZn, Au₅Zn₃, δ -Au₁₁Zn₁₄, and γ_2 -AuIn₃) are described by the two-sublattice model, while those of γ -Au₉In₄, ψ -Au₃In₂, α_1 -Au₃Zn, α_3 -Au₃Zn, and γ_3 -AuZn₃ are expressed by the three-sublattice model. In this research, the molar Gibbs energy of the γ_1 -AuZn₃ phase is modeled using a four-sublattice approach, whereas the α (Au, In) and ϵ_1 -Au₃Zn₁₇ intermetallic compounds are characterized through the substitutional solution model. Owing to an absence of experimental data, the solubility of Ge within the Au-In, Au-Sb, and Au-Zn intermetallic compounds has not been included in the thermodynamic assessments for the Au-Ge-In, Au-Ge-Sb, and Au-Ge-Zn systems. The Gibbs energy values for these binary intermetallic compounds are derived from studies by Liu et al. [26,31,40]. Thermodynamic models of these Au-In, Au-Sb, and Au-Zn binary intermetallic compounds were shown completely in Refs. [26,31,40] and, thus, are not duplicated here.

4. Calculated Results and Discussion

Leveraging the lattice stabilities compiled by Dinsdale [24], the optimization of thermodynamic parameters for the Au-Ge-X (X = In, Sb, Si, Zn) systems was performed using the PARROT module within the Thermo-Calc[®] software 2024a, as developed by Sundman et al. [44]. The final results, detailing the thermodynamic parameters for all phases within these systems, are comprehensively presented across Tables 2–5.

Table 2. Thermodynamic parameters for the Au-Ge-In system.

Phase	Thermodynamic Parameters	Reference
liquid (Au, Ge, In)	${}^0L_{Au,Ge}^{liq} = -18,294.684 - 13.671T$ ${}^1L_{Au,Ge}^{liq} = -8894.639 - 6.339T$	[14]
	${}^2L_{Au,Ge}^{liq} = -2174.476 - 4.925T$	[14]
	${}^0L_{Au,In}^{liq} = -76,196.19 + 64.291T - 6.638T \ln T$	[26]
	${}^1L_{Au,In}^{liq} = -31,134.02 + 81.358T - 8.513T \ln T$	[26]
	${}^0L_{Ge,In}^{liq} = +1587.2 - 0.3871T$ ${}^1L_{Ge,In}^{liq} = -583.5 - 1.511T$	[26]
	${}^0L_{Au,Ge,In}^{liq} = +62,816.812$ ${}^1L_{Au,Ge,In}^{liq} = +53443.685$ ${}^2L_{Au,Ge,In}^{liq} = -23278.378$	This work
fcc (Au, Ge, In)	${}^0L_{Au,Ge}^{fcc} = +10,198.859 - 23.114T$	[14]
	${}^0L_{Au,In}^{fcc} = -48,493.65 + 46.624T - 6.831T \ln T$	[26]
	${}^1L_{Au,In}^{fcc} = +498.45$	[26]
diamond(Ge)	${}^0C_{Ge}^{dia}$ cited from SGTE database	[14]
tetragonal(In)	${}^0C_{In}^{tetr.}$ cited from SGTE database	[26]
hcp(Au, In)	${}^0L_{Au,In}^{hcp} = -55,780.55 + 13.820T$ ${}^1L_{Au,In}^{hcp} = +6788.95 - 32.894T$	[26]

Table 2. Cont.

Phase	Thermodynamic Parameters	Reference
$\alpha(\text{Au, In})$	${}^0L_{\text{Au,In}}^\alpha = -48,238.66 + 5.355T$ ${}^1L_{\text{Au,In}}^\alpha = -48.36 - 16.793T$	[26]
$\beta\text{-Au}_4\text{In}$	$G_{\text{Au:In}}^{\beta\text{-Au}_4\text{In}} = -8980.42 - 3.304T + 0.785{}^0G_{\text{Au}}^{\text{fcc}} + 0.215{}^0G_{\text{In}}^{\text{tetr.}}$	[26]
$\beta'\text{-Au}_4\text{In}$	$G_{\text{Au:In}}^{\beta'\text{-Au}_4\text{In}} = -9382.52 - 3.102T + 0.778{}^0G_{\text{Au}}^{\text{fcc}} + 0.222{}^0G_{\text{In}}^{\text{tetr.}}$	[26]
$\gamma\text{-Au}_9\text{In}_4$	$G_{\text{Au:Au:In}}^{\gamma\text{-Au}_9\text{In}_4} = -2830.47 - 2.519T + 0.923{}^0G_{\text{Au}}^{\text{fcc}} + 0.077{}^0G_{\text{In}}^{\text{tetr.}}$	[26]
	$G_{\text{Au:In:In}}^{\gamma\text{-Au}_9\text{In}_4} = -11,992.16 - 3.651T + 0.692{}^0G_{\text{Au}}^{\text{fcc}} + 0.308{}^0G_{\text{In}}^{\text{tetr.}}$	[26]
	$L_{\text{Au:Au,In:In}}^{\gamma\text{-Au}_9\text{In}_4} = +2144.6$	[26]
$\gamma'\text{-Au}_7\text{In}_3$	$G_{\text{Au:In}}^{\gamma'\text{-Au}_7\text{In}_3} = -12,813.11 - 2.054T + 0.7{}^0G_{\text{Au}}^{\text{fcc}} + 0.3{}^0G_{\text{In}}^{\text{tetr.}}$	[26]
$\psi\text{-Au}_3\text{In}_2$	$G_{\text{Au:Au:In}}^{\psi\text{-Au}_3\text{In}_2} = +2153.38 - 8.039T + 0.833{}^0G_{\text{Au}}^{\text{fcc}} + 0.167{}^0G_{\text{In}}^{\text{tetr.}}$	[26]
	$G_{\text{Au:In:In}}^{\psi\text{-Au}_3\text{In}_2} = -18,225.14 - 3.0T + 0.5{}^0G_{\text{Au}}^{\text{fcc}} + 0.5{}^0G_{\text{In}}^{\text{tetr.}}$	[26]
	$L_{\text{Au:Au,In:In}}^{\psi\text{-Au}_3\text{In}_2} = -15,683.16$	[26]
Au_3In	$G_{\text{Au:In}}^{\text{Au}_3\text{In}} = -10,582.67 - 2.932T + 0.75{}^0G_{\text{Au}}^{\text{fcc}} + 0.25{}^0G_{\text{In}}^{\text{tetr.}}$	[26]
AuIn	$G_{\text{Au:In}}^{\text{AuIn}} = -20,188.37 + 2.379T + 0.5{}^0G_{\text{Au}}^{\text{fcc}} + 0.5{}^0G_{\text{In}}^{\text{tetr.}}$	[26]
AuIn_2	$G_{\text{Au:In}}^{\text{AuIn}_2} = -26,129.06 + 11.113T + 0.333{}^0G_{\text{Au}}^{\text{fcc}} + 0.667{}^0G_{\text{In}}^{\text{tetr.}}$	[26]

Table 3. Thermodynamic parameters for the Au-Ge-Sb system.

Phase	Thermodynamic Parameters	Reference
liquid (Au, Ge, Sb)	${}^0L_{\text{Au,Ge}}^{\text{liq}} = -18,294.684 - 13.671T$ ${}^1L_{\text{Au,Ge}}^{\text{liq}} = -8894.639 - 6.339T$	[14]
	${}^2L_{\text{Au,Ge}}^{\text{liq}} = -2174.476 - 4.925T$	[14]
	${}^0L_{\text{Au,Sb}}^{\text{liq}} = -15,067.47 + 23.15424T - 4.988235T \ln T$	[31]
	${}^1L_{\text{Au,Sb}}^{\text{liq}} = -2427.37 - 8.3278T$	[31]
	${}^0L_{\text{Ge,Sb}}^{\text{liq}} = +3289.7 - 0.521T$	[21]
	${}^0L_{\text{Au,Ge,Sb}}^{\text{liq}} = -22,395.305$	This work
	${}^1L_{\text{Au,Ge,Sb}}^{\text{liq}} = +11,801.969$	This work
	${}^2L_{\text{Au,Ge,Sb}}^{\text{liq}} = +17,008.798$	This work
fcc (Au, Ge, Sb)	${}^0L_{\text{Au,Ge}}^{\text{fcc}} = +10,198.859 - 23.114T$	[14]
	${}^0L_{\text{Au,Sb}}^{\text{fcc}} = +24,512.703 - 25T$	[31]
diamond (Ge, Sb)	${}^0L_{\text{Ge,Sb}}^{\text{dia.}} = +79210.1 - 19.8T$	[21]
rhombohedral (Ge, Sb)	${}^0L_{\text{Au,Sb}}^{\text{rho.}} = +3000 - 0.1T$	[31]
	${}^0L_{\text{Ge,Sb}}^{\text{rho.}} = +10,695 - 6.557T$	[21]
AuSb_2	$G_{\text{Au:Sb}}^{\text{AuSb}_2} = -5450.31 + 12.8064T - 1.63691T \ln T + 0.333{}^0G_{\text{Au}}^{\text{fcc}} + 0.667{}^0G_{\text{Sb}}^{\text{rho.}}$	[31]

Table 4. Thermodynamic parameters for the Au-Ge-Si system.

Phase	Thermodynamic Parameters	Reference
liquid (Au, Ge, Si)	${}^0L_{Au,Ge}^{liq} = -18,294.684 - 13.671T$	[14]
	${}^1L_{Au,Ge}^{liq} = -8894.639 - 6.339T$	[14]
	${}^2L_{Au,Ge}^{liq} = -2174.476 - 4.925T$	[14]
	${}^0L_{Au,Si}^{liq} = -24,103.303 - 15.139T$	[20]
	${}^1L_{Au,Si}^{liq} = -29,375.278 + 1.107T$	[20]
	${}^2L_{Au,Si}^{liq} = -13,032.241$	[20]
	${}^0L_{Ge,Si}^{liq} = +6000$	[35]
	${}^0L_{Au,Ge,Si}^{liq} = -26,000$	This work
	${}^1L_{Au,Ge,Si}^{liq} = +70,000$	This work
	${}^2L_{Au,Ge,Si}^{liq} = +48,000$	This work
fcc (Au, Ge, Si)	${}^0L_{Au,Ge}^{fcc} = +10,198.859 - 23.114T$	[14]
	${}^0L_{Au,Si}^{fcc} = +2000$	[20]
diamond (Au, Ge, Si)	${}^0L_{Au,Si}^{dia.} = +40,000$	[20]
	${}^0L_{Ge,Si}^{dia.} = +3500$	[35]

Table 5. Thermodynamic parameters for the Au-Ge-Zn system.

Phase	Thermodynamic Parameters	Reference
liquid (Au, Ge, Zn)	${}^0L_{Au,Ge}^{liq} = -18,294.684 - 13.671T,$	[14]
	${}^1L_{Au,Ge}^{liq} = -8894.639 - 6.339T, {}^2L_{Au,Ge}^{liq} = -2174.476 - 4.925T$	
	${}^0L_{Au,Zn}^{liq} = -96,492.26 + 42.713T - 3.041T \ln T, {}^1L_{Au,Zn}^{liq} = -5576.71 + 0.015T$	[40]
	${}^0L_{Ge,Zn}^{liq} = +4940.9 - 6.510T, {}^1L_{Ge,Zn}^{liq} = +1119$	[27]
	${}^0L_{Au,Ge,Zn}^{liq} = +10,000, {}^1L_{Au,Ge,Zn}^{liq} = +50,000, {}^2L_{Au,Ge,Zn}^{liq} = +100,000$	This work
fcc (Au, Ge, Zn)	${}^0L_{Au,Ge}^{fcc} = +10198.859 - 23.114T$	[14]
	${}^0L_{Au,Zn}^{fcc} = -95,112.59 + 101.687T - 11.897T \ln T, {}^1L_{Au,Zn}^{fcc} = +452.29 + 7.540T$	[40]
Diamond (Ge, Zn)	${}^0L_{Ge,Zn}^{dia.} = +80T$	[27]
hcp(Au, Zn)	${}^0L_{Au,Zn}^{hcp} = -49193.15 + 11.770T, {}^1L_{Au,Zn}^{hcp} = +21,680.4$	[40]
α_1 -Au ₃ Zn	$G_{Au:Au_3Zn}^{\alpha_1-Au_3Zn} = -78,040.1 + 11.236T + 4{}^0G_{Au}^{fcc} + 0{}G_{Zn}^{hcp}$	[40]
	$G_{Au:Zn_3Zn}^{\alpha_1-Au_3Zn} = -120,613.65 + 31.264T + 3{}^0G_{Au}^{fcc} + 2{}^0G_{Zn}^{hcp}$	[40]
	$L_{Au:Au_3Zn}^{\alpha_1-Au_3Zn} = -31715.85 + 16.239T$	[40]
α_2 -Au ₃ Zn	$G_{Au:Zn}^{\alpha_2-Au_3Zn} = -19,009 + 3.074T + 0.75{}^0G_{Au}^{fcc} + 0.25{}^0G_{Zn}^{hcp}$	[40]
α_3 -Au ₃ Zn	$G_{Au:Au_3Zn}^{\alpha_3-Au_3Zn} = -260,713.32 + 72.188T + 25{}^0G_{Au}^{fcc} + 3{}^0G_{Zn}^{hcp}$	[40]
	$G_{Au:Zn_3Zn}^{\alpha_3-Au_3Zn} = -624,105.44 + 152.293T + 18{}^0G_{Au}^{fcc} + 10{}^0G_{Zn}^{hcp}$	[40]
	$L_{Au:Au_3Zn}^{\alpha_3-Au_3Zn} = -202,141.24 + 16.494T$	[40]
ε_1 -Au ₃ Zn ₁₇	${}^0L_{Au,Zn}^{\varepsilon_1-Au_3Zn_{17}} = -82,852.97 + 26.406T, {}^1L_{Au,Zn}^{\varepsilon_1-Au_3Zn_{17}} = +58047.97 - 20.171T$	[40]
ε_2 -Au ₃ Zn ₁₇	$G_{Au:Zn}^{\varepsilon_2-Au_3Zn_{17}} = -12620 + 0.166T + 0.15{}^0G_{Au}^{fcc} + 0.85{}^0G_{Zn}^{hcp}$	[40]

Table 5. Cont.

Phase	Thermodynamic Parameters	Reference
β_1 -AuZn	$G_{Au:Zn}^{\beta_1-AuZn} = G_{Zn:Au}^{\beta_1-AuZn} = -82,852.97 + 26.40577T$	[40]
	$L_{Au,Zn:Zn}^{\beta_1-AuZn} = L_{Zn:Au,Zn}^{\beta_1-AuZn} = +58,047.97 - 20.17125T$	[40]
Au_5Zn_3	$G_{Au:Zn}^{Au_5Zn_3} = -192,392.71 + 32.154T + 5^0G_{Au}^{fcc} + 3^0G_{Zn}^{hcp}$	[40]
δ_1 - $Au_{11}Zn_{14}$	$G_{Au:Zn}^{\delta_1-Au_{11}Zn_{14}} = -618815.02 + 25.913T + 11^0G_{Au}^{fcc} + 14^0G_{Zn}^{hcp}$	[40]
γ_1 - $AuZn_3$	$G_{Au:Au:Au:Zn}^{\gamma_1-AuZn_3} = -255,281.18 + 13.147T + 7^0G_{Au}^{fcc} + 6^0G_{Zn}^{hcp}$	[40]
	$G_{Zn:Au:Au:Zn}^{\gamma_1-AuZn_3} = -149,825.99 + 2.318T + 5^0G_{Au}^{fcc} + 8^0G_{Zn}^{hcp}$	[40]
	$G_{Au:Au:Zn:Zn}^{\gamma_1-AuZn_3} = -273,238.57 + 6.566T + 4^0G_{Au}^{fcc} + 9^0G_{Zn}^{hcp}$	[40]
	$G_{Zn:Au:Zn:Zn}^{\gamma_1-AuZn_3} = -154,065 + 20.830T + 2^0G_{Au}^{fcc} + 11^0G_{Zn}^{hcp}$	[40]
	$L_{Au,Zn:Au:Au:Zn}^{\gamma_1-AuZn_3} = L_{Au,Zn:Au:Zn:Zn}^{\gamma_1-AuZn_3} = -58,164.63,$	[40]
	$L_{Au:Au:Au,Zn:Zn}^{\gamma_1-AuZn_3} = L_{Zn:Au:Au,Zn:Zn}^{\gamma_1-AuZn_3} = -107,389.21$	[40]
γ_2 - $AuZn_3$	$G_{Au:Zn}^{\gamma_2-AuZn_3} = -78,726.23 + 5.314T + 0G_{Au}^{Fcc} + 3^0G_{Zn}^{Hcp}$	[40]
γ_3 - $AuZn_3$	$G_{Au:Au:Zn}^{\gamma_3-AuZn_3} = -20,516.36 + 1.969T + 0.28^0G_{Au}^{fcc} + 0.72^0G_{Zn}^{hcp}$	[40]
	$G_{Au:Zn:Zn}^{\gamma_3-AuZn_3} = -9775.48 + 0.028T + 0.12^0G_{Au}^{fcc} + 0.88^0G_{Zn}^{hcp}$	[40]
	$L_{Au:Au,Zn:Zn}^{\gamma_3-AuZn_3} = -3445.87$	[40]

4.1. The Au-Ge-In System

In this study, Figure 1 depicts the liquidus projection for the Au-Ge-In system. Additionally, Figure 2 outlines the reaction scheme for this system.

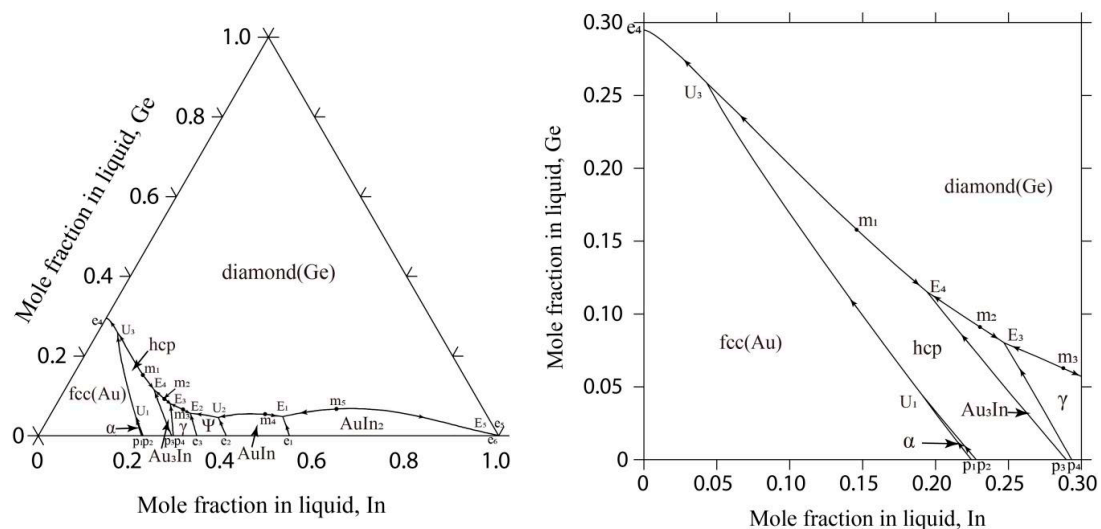


Figure 1. The calculated liquidus projection of the Au-Ge-In system in this study.

It can be seen in Figure 1 that there are five E-type invariant reactions (E_1 : Liquid \leftrightarrow diamond(Ge) + AuIn + AuIn₂ at 747 K, E_2 : Liquid \leftrightarrow diamond(Ge) + γ -Au₉In₄ + ψ -Au₃In₂ at 671 K, E_3 : Liquid \leftrightarrow diamond(Ge) + γ -Au₉In₄ + Au₃In at 667 K, E_4 : Liquid \leftrightarrow diamond(Ge) + hcp(Au, In) + Au₃In at 665 K, E_5 : Liquid \leftrightarrow diamond(Ge) + AuIn₂ + tetragonal(In) at 429 K) and three U-type invariant reactions (U_1 : Liquid + α (Au, In) \leftrightarrow fcc(Au) + hcp(Au, In) at 863 K, U_2 : Liquid + AuIn \leftrightarrow diamond(Ge) + ψ -Au₃In₂ at 694 K, U_3 : Liquid + hcp(Au, In) \leftrightarrow diamond(Ge) + fcc(Au) at 654 K). The calculated temperature and composition of E_1 (747 K, 44.4 at.% Au-4.8 at.% Ge) are in good accordance with the experimental results (744 K, 43.3 at.% Au-3.5 at.% Ge) [28]. The calculated temperature of E_5 in the rich In part is 429 K, which is well consistent with the reported value (429 K) [28].

Furthermore, it was observed in Figures 1 and 2 that there are five maximum points (m_1 : 667 K, 69.6 at.% Au-15.8 at.% Ge; m_2 : 668 K, 67.9 at.% Au-9.1 at.% Ge; m_3 : 673 K, 64.9 at.% Au-6.3 at.% Ge; m_4 : 751 K, 47.4 at.% Au-5.3 at.% Ge; m_5 : 790 K, 31.0 at.% Au-6.7 at.% Ge) located on the monovariant curves of U_3 - E_4 , E_4 - E_3 , E_3 - E_2 , U_2 - E_1 , and E_1 - E_5 , which needs to be verified by the further experimental investigations.

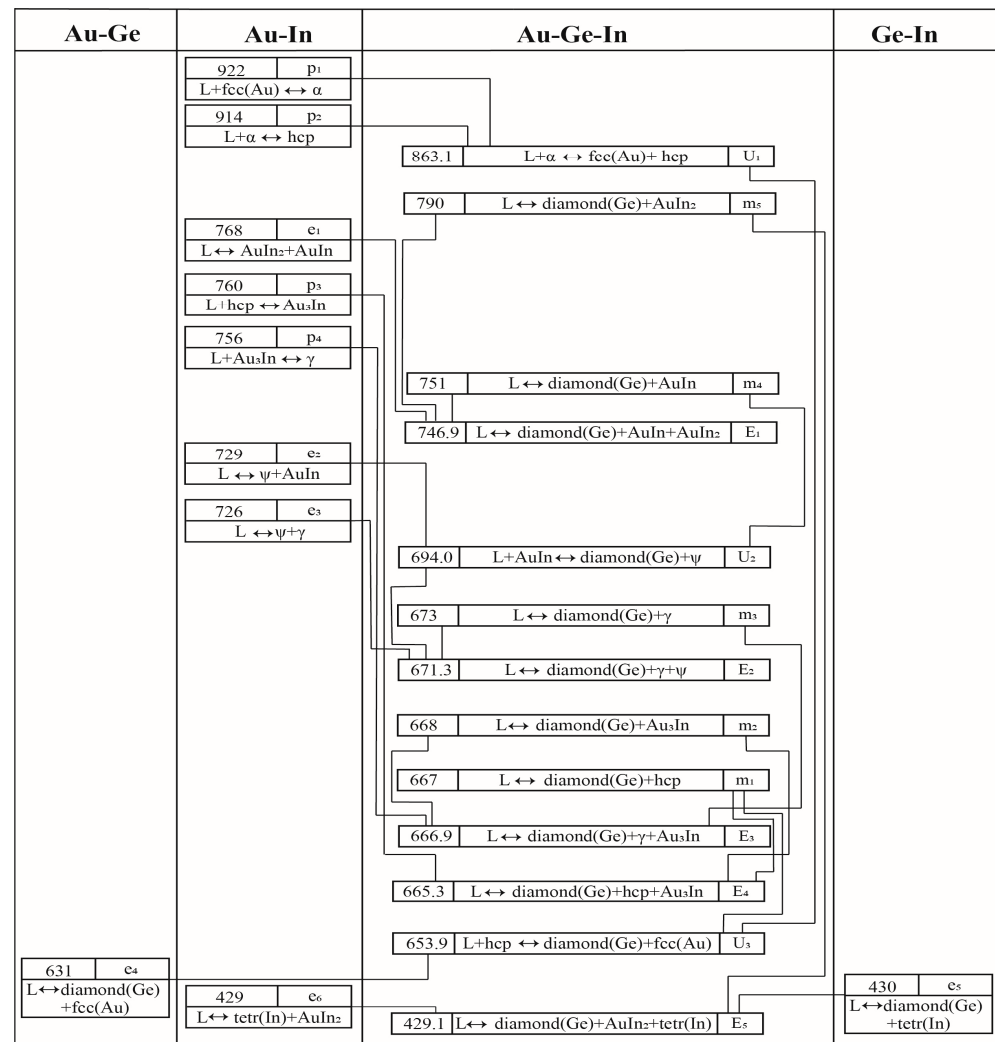


Figure 2. Reaction scheme of the Au-Ge-In system.

Table 6 displays the results from the invariant reactions in the Au-Ge-In system, including temperatures and compositions, which align with the experimental findings detailed in reference [28].

Figure 3 compares the calculated four vertical sections of AuIn-Ge, Au_{41.5}In_{58.5}-Ge, AuIn₂-Ge, and Au₂₀In₈₀-Ge with the experimental results [28]. As can be seen, these four vertical sections display a pseudo-binary eutectic characteristic. In Figure 3a, the calculated transition temperature and the composition of the liquid phase for the AuIn-Ge vertical section are 764 K and 3.0 at.% Ge, which are consistent with the experimental results (761 K and 2.0 at.% Ge) [28], respectively.

Table 6. Invariant reactions in the Au-Ge-In system.

Invariant Reactions	Type	T (K)	Composition		Reference
			x_{Au}^{L}	x_{Ge}^{L}	
$\text{L} + \alpha(\text{Au, In}) \leftrightarrow \text{fcc}(\text{Au}) + \text{hcp}(\text{Au, In})$	U ₁	863	0.765	0.045	This work
$\text{L} \leftrightarrow \text{diamond}(\text{Ge}) + \text{AuIn} + \text{AuIn}_2$	E ₁	747 744	0.444 0.433	0.048 0.035	This work [28]
$\text{L} + \text{AuIn} \leftrightarrow \text{diamond}(\text{Ge}) + \psi\text{-Au}_3\text{In}_2$	U ₂	964	0.586	0.046	This work
$\text{L} \leftrightarrow \text{diamond}(\text{Ge}) + \gamma\text{-Au}_9\text{In}_4 + \psi\text{-Au}_3\text{In}_2$	E ₂	671	0.641	0.056	This work
$\text{L} \leftrightarrow \text{diamond}(\text{Ge}) + \gamma\text{-Au}_9\text{In}_4 + \text{Au}_3\text{In}$	E ₃	667	0.673	0.080	This work
$\text{L} \leftrightarrow \text{diamond}(\text{Ge}) + \text{hcp}(\text{Au, In}) + \text{Au}_3\text{In}$	E ₄	665	0.691	0.115	This work
$\text{L} + \text{hcp}(\text{Au, In}) \leftrightarrow \text{diamond}(\text{Ge}) + \text{fcc}(\text{Au})$	U ₃	654	0.698	0.259	This work
$\text{L} \leftrightarrow \text{diamond}(\text{Ge}) + \text{AuIn}_2 + \text{tetragonal}(\text{In})$	E ₅	429 429	0.001 —	0.001 —	This work [28]
$\text{L} \leftrightarrow \text{diamond}(\text{Ge}) + \text{hcp}(\text{Au, In})$	m ₁	667	0.696	0.158	This work
$\text{L} \leftrightarrow \text{diamond}(\text{Ge}) + \text{Au}_3\text{In}$	m ₂	668	0.679	0.091	This work
$\text{L} \leftrightarrow \text{diamond}(\text{Ge}) + \gamma\text{-Au}_9\text{In}_4$	m ₃	673	0.649	0.063	This work
$\text{L} \leftrightarrow \text{diamond}(\text{Ge}) + \text{AuIn}$	m ₄	751	0.474	0.053	This work
$\text{L} \leftrightarrow \text{diamond}(\text{Ge}) + \text{AuIn}_2$	m ₅	790	0.310	0.067	This work

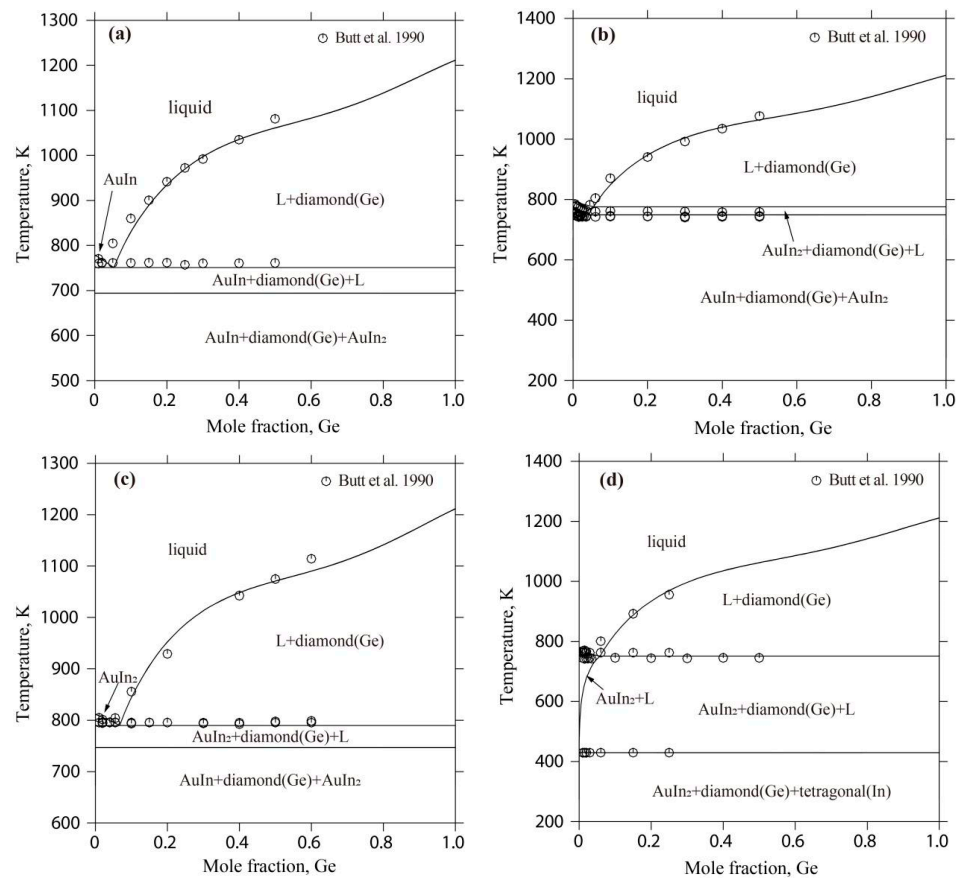


Figure 3. Calculated vertical sections of the Au-Ge-In system with the experimental results [28]: (a) AuIn-Ge; (b) Au_{41.5}In_{58.5}-Ge; (c) AuIn₂-Ge; and (d) Au₂₀In₈₀-Ge.

Specifically, in panel (a) of Figure 3, the transition temperature and the composition of the liquid phase for the AuIn-Ge section were determined to be 764 K and 3.0 atomic percent Ge, aligning closely with the experimental values of 761 K and 2.0 atomic percent Ge [28]. Panels (b), (c), and (d) of Figure 3 show that the results for the Au_{41.5}In_{58.5}-Ge, AuIn₂-Ge, and Au₂₀In₈₀-Ge sections also correspond well with the experimental findings [28]. The calculated liquidus in these sections within the Au-Ge-In system demonstrates good agreement with the documented experimental results [28].

4.2. The Au-Ge-Sb System

Figure 4 displays the liquidus projection for the Au-Ge-Sb system calculated in this study, alongside comparisons to the projections made by Wang et al. [15]. Figure 5 depicts the reaction scheme derived from the current calculations for the same system. Additionally, Table 7 lists the temperatures and compositions for the invariant reactions within the Au-Ge-Sb system, validated against both experimental findings [33] and previous calculations [15]. As shown in Figure 4, the liquidus projection of the Au-Ge-Sb system includes one E-type invariant reaction (E₁: Liquid ↔ diamond(Ge) + fcc(Au) + AuSb₂) and one U-type invariant reaction (U₁: Liquid + rhombohedra(Sb) ↔ diamond(Ge) + AuSb₂). In this work, the temperatures of these two invariant reactions were calculated to be 561 K and 703 K, which are consistent well with the experimental data (561 K and 703 K) measured by Zwingmann [33]. The calculated results of this work are much better than the results (560 K and 702 K) of Wang et al. [15]. Moreover, the compositions of the liquid phase for these two invariant reactions were calculated to be 64.1 at.% Au-16.6 at.% Ge and 38.0 at.% Au-13.7 at.% Ge, which are consistent with the experimental data (68.0 at.% Au-15.0 at.% Ge and 35.0 at.% Au-14.0 at.% Ge) [33] and the calculated results [15].

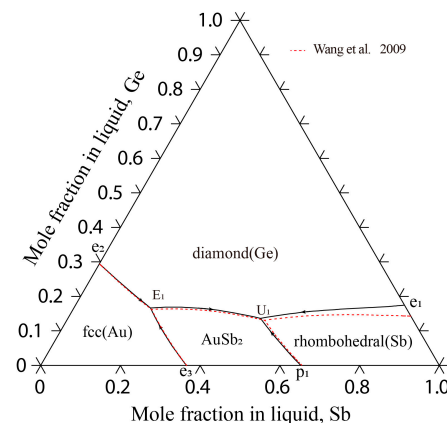


Figure 4. Calculated liquidus projection of the Au-Ge-Sb system in this study with the calculated results by Wang et al. [15].

Table 7. Invariant reactions in the Au-Ge-Sb system.

Invariant Reactions	Type	T (K)	Composition		Reference
			x_{Au}^{L}	x_{Ge}^{L}	
L + rhombohedral (Sb) ↔ diamond (Ge) + AuSb ₂	U ₁	703	0.350	0.140	[33]
		702	0.383	0.137	[15]
		703	0.379	0.137	This work
L ↔ diamond (Ge) + fcc (Au) + AuSb ₂	E ₁	561	0.680	0.150	[33]
		560	0.639	0.166	[15]
		561	0.641	0.166	This work

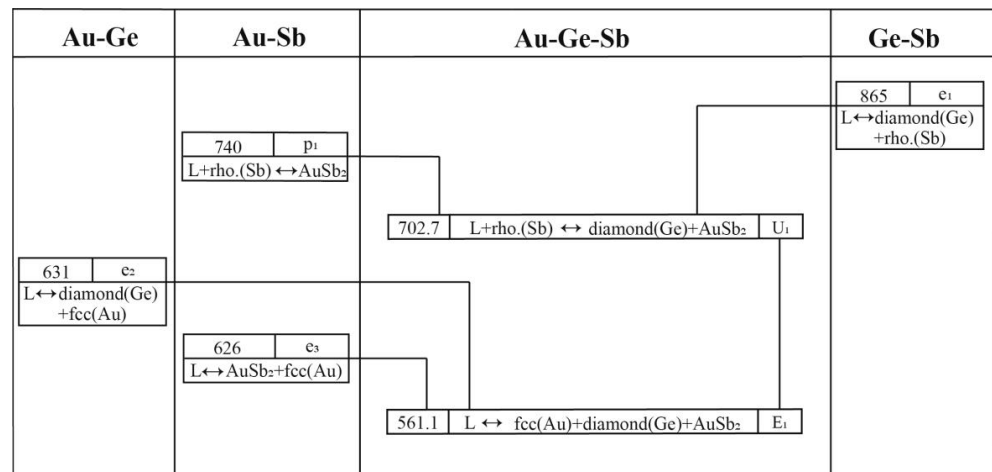


Figure 5. Reaction scheme of the Au-Ge-Sb system.

Figure 6 presents the calculated vertical sections of Au-Ge_{0.1}Sb_{0.9}, AuSb₂-Ge, and 15 at.% Ge, compared against both the experimental findings [33] and the previously calculated results [15]. Panels (a) and (c) of Figure 6 reveal that the phase-transition temperatures and liquidus lines for the Au-Ge_{0.1}Sb_{0.9} and 15 atomic percent Ge sections align closely with the experimental data [33]. For the AuSb₂-Ge section, the calculated liquidus corresponds with the calculated data [15] but exhibits a minor variance from the experimental observations [33].

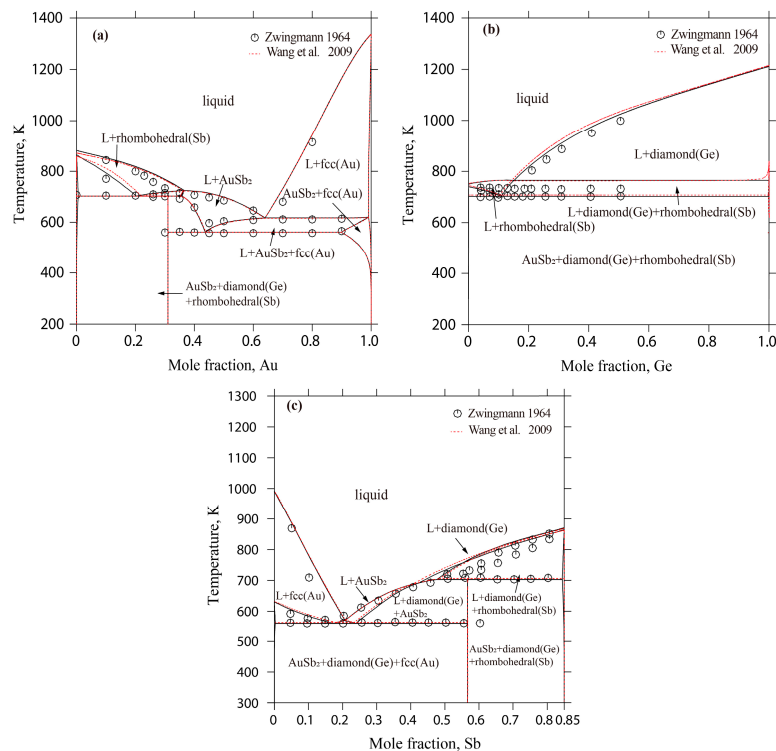


Figure 6. Calculated vertical sections of the Au-Ge-Sb system with the experimental results [33] and the calculated results [15]: (a) Au-Ge_{0.1}Sb_{0.9}; (b) AuSb₂-Ge; and (c) 15 at.% Ge.

4.3. The Au-Ge-Si Ternary System

The calculated liquidus projection of the Au-Ge-Si system is shown in Figure 7; the Au-Ge-Si system presents a monotropic eutectic reaction including the liquid phase, fcc(Au) and diamond(Ge, Si). The monovariant curve from the Au-Si binary eutectic point e₁ to

the Au-Ge binary eutectic point e_2 passes smoothly through a minimum point (599 K and 13.8 at.% Ge-11.7 at.% Si), which is consistent with the reported data (599 K and 8.8 at.% Ge-13.2 at.% Si) by Predel et al. [37].

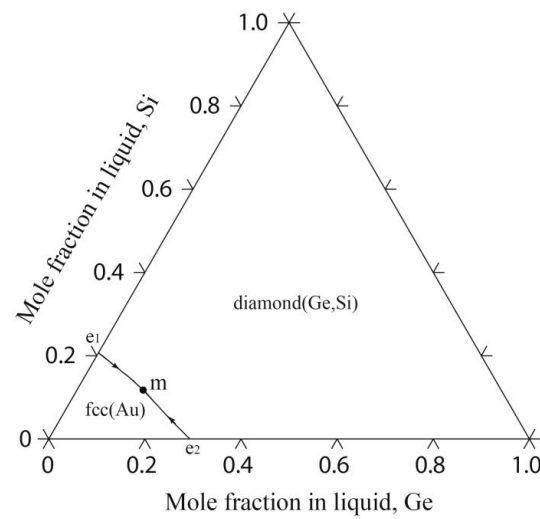


Figure 7. Calculated liquidus projection of the Au-Ge-Si system in this study.

Comparing the experimental data and the calculated results of the four vertical sections of Au-Ge_{0.8}Si_{0.2}, Au-Ge_{0.6}Si_{0.4}, Au-Ge_{0.4}Si_{0.6}, and Au-Ge_{0.2}Si_{0.8}, the calculated liquidus temperatures and phase-transition temperatures for the four vertical sections match the experimental data well, as shown in Figure 8. All the four vertical sections present a pseudo-binary eutectic characteristic [37].

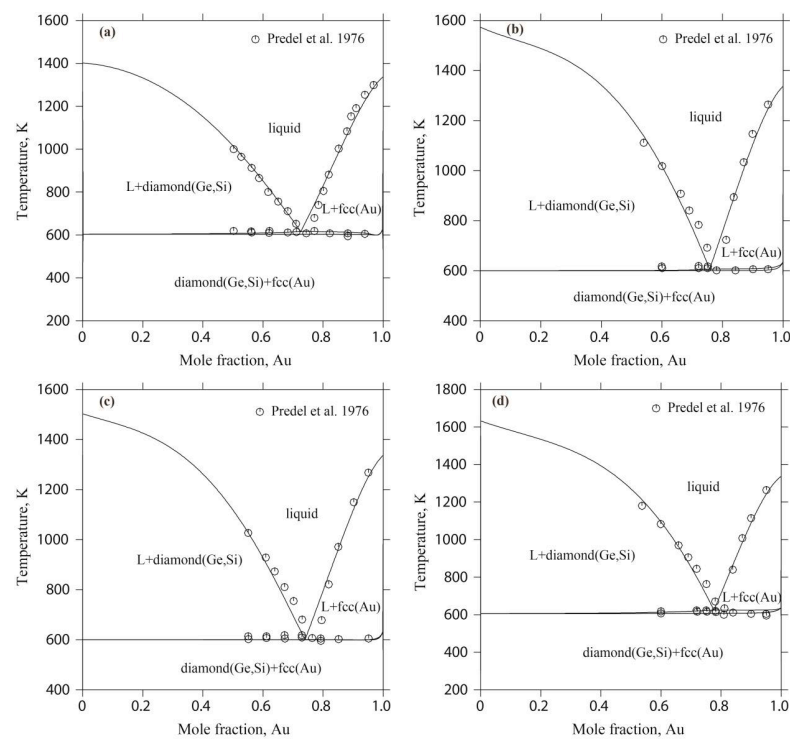


Figure 8. Calculated vertical sections of the Au-Ge-Si system with the experimental results [37]: (a) Au-Ge_{0.8}Si_{0.2}; (b) Au-Ge_{0.4}Si_{0.6}; (c) Au-Ge_{0.6}Si_{0.4}; and (d) Au-Ge_{0.2}Si_{0.8}.

4.4. The Au-Ge-Zn Ternary System

Figure 9 illustrates the reaction scheme of this system as obtained in this study, and Figure 10 shows the liquidus projection of the Au-Ge-Zn system that was calculated. Table 8 provides a summary of the temperatures and compositions of the invariant reactions.

Au-Ge	Au-Zn	Au-Ge-Zn	Ge-Zn													
	<table border="1"> <tr><td>953</td><td>e₁</td></tr> <tr><td colspan="2">L ↔ β₂+fcc(Au)</td></tr> </table>	953	e ₁	L ↔ β ₂ +fcc(Au)												
953	e ₁															
L ↔ β ₂ +fcc(Au)																
	<table border="1"> <tr><td>946</td><td>e₂</td></tr> <tr><td colspan="2">L ↔ β₂+γ₁</td></tr> </table>	946	e ₂	L ↔ β ₂ +γ ₁		<table border="1"> <tr><td>943.6</td><td>L ↔ diamond(Ge)+β₂</td><td>m₁</td></tr> <tr><td>928.2</td><td>L ↔ diamond(Ge)+γ₁</td><td>m₂</td></tr> <tr><td>919.6</td><td>L ↔ diamond(Ge)+β₂+γ₁</td><td>E₁</td></tr> </table>	943.6	L ↔ diamond(Ge)+β ₂	m ₁	928.2	L ↔ diamond(Ge)+γ ₁	m ₂	919.6	L ↔ diamond(Ge)+β ₂ +γ ₁	E ₁	
946	e ₂															
L ↔ β ₂ +γ ₁																
943.6	L ↔ diamond(Ge)+β ₂	m ₁														
928.2	L ↔ diamond(Ge)+γ ₁	m ₂														
919.6	L ↔ diamond(Ge)+β ₂ +γ ₁	E ₁														
	<table border="1"> <tr><td>855</td><td>p₁</td></tr> <tr><td colspan="2">L+γ₁ ↔ γ₃</td></tr> </table>	855	p ₁	L+γ ₁ ↔ γ ₃		<table border="1"> <tr><td>841.4</td><td>L+γ₁ ↔ diamond(Ge)+γ₃</td><td>U₁</td></tr> </table>	841.4	L+γ ₁ ↔ diamond(Ge)+γ ₃	U ₁							
855	p ₁															
L+γ ₁ ↔ γ ₃																
841.4	L+γ ₁ ↔ diamond(Ge)+γ ₃	U ₁														
	<table border="1"> <tr><td>763</td><td>p₂</td></tr> <tr><td colspan="2">L+γ₃ ↔ ε₁</td></tr> </table>	763	p ₂	L+γ ₃ ↔ ε ₁		<table border="1"> <tr><td>801.6</td><td>L+β₂ ↔ diamond(Ge)+fcc(Au)</td><td>U₂</td></tr> <tr><td>747.4</td><td>L+γ₃ ↔ diamond(Ge)+ε₁</td><td>U₃</td></tr> </table>	801.6	L+β ₂ ↔ diamond(Ge)+fcc(Au)	U ₂	747.4	L+γ ₃ ↔ diamond(Ge)+ε ₁	U ₃				
763	p ₂															
L+γ ₃ ↔ ε ₁																
801.6	L+β ₂ ↔ diamond(Ge)+fcc(Au)	U ₂														
747.4	L+γ ₃ ↔ diamond(Ge)+ε ₁	U ₃														
	<table border="1"> <tr><td>718</td><td>p₃</td></tr> <tr><td colspan="2">L+ε₁ ↔ hcp(Zn)</td></tr> </table>	718	p ₃	L+ε ₁ ↔ hcp(Zn)		<table border="1"> <tr><td>693.3</td><td>L+ε₁ ↔ diamond(Ge)+hcp(Zn)</td><td>U₄</td></tr> </table>	693.3	L+ε ₁ ↔ diamond(Ge)+hcp(Zn)	U ₄							
718	p ₃															
L+ε ₁ ↔ hcp(Zn)																
693.3	L+ε ₁ ↔ diamond(Ge)+hcp(Zn)	U ₄														
<table border="1"> <tr><td>631</td><td>e₄</td></tr> <tr><td colspan="2">L ↔ diamond(Ge)+fcc(Au)</td></tr> </table>	631	e ₄	L ↔ diamond(Ge)+fcc(Au)			<table border="1"> <tr><td>665</td><td>e₃</td></tr> <tr><td colspan="2">L ↔ diamond(Ge)+hcp(Zn)</td></tr> </table>	665	e ₃	L ↔ diamond(Ge)+hcp(Zn)							
631	e ₄															
L ↔ diamond(Ge)+fcc(Au)																
665	e ₃															
L ↔ diamond(Ge)+hcp(Zn)																

Figure 9. Reaction scheme of the Au-Ge-Zn system.

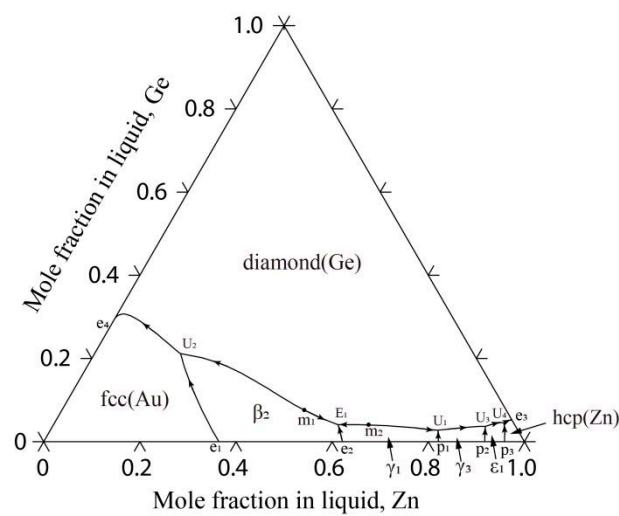


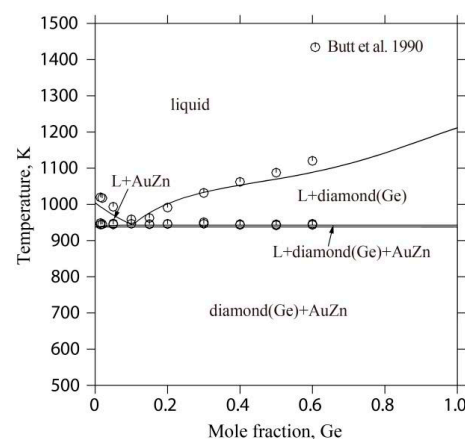
Figure 10. Calculated liquidus projection of the Au-Ge-Zn system in this study.

Table 8. Invariant reactions in the Au-Ge-Zn system.

Invariant Reactions	Type	T (K)	Composition		Reference
			x_{Au}^{L}	x_{Ge}^{L}	
$\text{L} \leftrightarrow \beta_2\text{-AuZn} + \text{diamond (Ge)} + \gamma_1\text{-AuZn}_3$	E ₁	920	0.368	0.041	This work
$\text{L} + \gamma_1\text{-AuZn}_3 \leftrightarrow \text{diamond (Ge)} + \gamma_3\text{-AuZn}$	U ₁	841	0.166	0.028	This work
$\text{L} + \beta_2\text{-AuZn} \leftrightarrow \text{diamond (Ge)} + \text{fcc (Au)}$	U ₂	802	0.610	0.211	This work
$\text{L} + \gamma_3\text{-AuZn} \leftrightarrow \text{diamond (Ge)} + \varepsilon_1\text{-Au}_3\text{Zn}_{17}$	U ₃	747	0.063	0.037	This work
$\text{L} + \varepsilon_1\text{-Au}_3\text{Zn}_{17} \leftrightarrow \text{diamond (Ge)} + \text{hcp (Zn)}$	U ₄	693	0.020	0.045	This work
$\text{L} \leftrightarrow \text{diamond (Ge)} + \beta_2\text{-AuZn}$	m ₁	944	0.440	0.094	This work
$\text{L} \leftrightarrow \text{diamond (Ge)} + \gamma_1\text{-AuZn}_3$	m ₂	928	0.319	0.041	This work

It is obvious that the liquidus projection of the Au-Ge-Zn system contains one E-type invariant reaction (E₁: Liquid \leftrightarrow β_2 -AuZn + diamond(Ge) + γ_1 -AuZn₃ at 920 K) and four U-type invariant reactions (U₁: Liquid + γ_1 -AuZn₃ \leftrightarrow diamond(Ge) + γ_3 -AuZn at 841 K, U₂: Liquid + β_2 -AuZn \leftrightarrow diamond(Ge) + fcc (Au) at 802 K, U₃: Liquid + γ_3 -AuZn₃ \leftrightarrow diamond(Ge) + ε_1 -Au₃Zn₁₇ at 747 K, U₄: Liquid + ε_1 -Au₃Zn₁₇ \leftrightarrow diamond(Ge) + hcp (Zn) at 693 K). Moreover, the liquidus projection of the Au-Ge-Zn system illustrates that the presence of two maximum points (m₁: 944 K and 44.0 at.% Au-9.4 at.% Ge; m₂: 928 K and 31.9 at.% Au-4.1 at.% Ge) that are located on the monovariant curves of E₁-U₂ and E₁-U₁. Because of the absence of experimental information on the liquidus projection of the Au-Ge-Zn system, additional experiments need to be performed to determine these invariant reactions and maximum points in the monovariant curves, which would be used to confirm the present calculations.

Figure 11 illustrates the computed vertical section of the AuZn-Ge system alongside the documented experimental outcomes [41]. This section exhibits characteristics of a pseudo-binary eutectic system. The study determined the eutectic reaction's temperature and composition at 943 K and 10.4 atomic percent Ge, aligning closely with the experimental measurements of 946 K and 12.2 atomic percent Ge [41]. Notably, the alignment of the calculated liquidus for this section with the experimental data [41] demonstrates the model's accuracy.

**Figure 11.** Calculated vertical sections of the Au-Ge-Zn system with the experimental results [41].

5. Conclusions

This study employed the CALPHAD approach, integrating it with data from the literature reviews and previous binary subsystem evaluations to conduct thermodynamic modeling of the Au-Ge-X (X = In, Sb, Si, Zn) systems. The comparison of the calculated liquidus projections and vertical sections of the Au-Ge-X (X = In, Sb, Si, Zn) systems

demonstrates that the present calculations are consistent with the reported experimental data. Finally, a set of available and self-consistent thermodynamic parameters of the Au-Ge-X ($X = \text{In, Sb, Si, Zn}$) systems was obtained. These parameters enable the prediction of phase equilibria and thermodynamic behaviors of the Au-Ge-X alloys. Such data are crucial for the development of a thermodynamic database for multi-component Au-based alloys, enhancing the exploration of innovative high-temperature lead-free solders for electronic applications.

Author Contributions: Y.B., M.R. and J.W. conceived and designed the calculations; Y.B., X.L. and Q.T. performed the calculations; Y.B., C.T. and M.L. collected and analyzed the data; Y.B., M.R. and J.W. wrote the paper. All authors have read and agreed to the published version of the manuscript.

Funding: This work was supported financially by the Innovation Project of Guangxi Graduate Education (YCSW2023321) and the Guangxi Key Laboratory of Information Materials, Guilin University of Electronic Technology, China (151009-Z).

Data Availability Statement: All the data that support the findings of this study are included within the article.

Conflicts of Interest: The authors declare no conflicts of interest.

References

1. Xu, J.; Wu, M.; Pu, J.; Xue, S. Novel Au-based solder alloys: A Potential Answer for Electrical Packaging Problem. *Adv. Mater. Sci. Eng.* **2020**, *2020*, 4969647. [[CrossRef](#)]
2. Wang, L.; Xue, S.; Liu, H.; Lin, Y.; Chen, H. Research Progress of Au-20Sn Solder for Electronic Packaging. *Cailiao Daobao* **2019**, *33*, 2483–2489.
3. Zhang, H.; Minter, J.; Lee, N.C. A brief review on high-temperature, Pb-free die-attach materials. *J. Electron. Mater.* **2019**, *48*, 201–210. [[CrossRef](#)]
4. Larsson, A.; Tollefsen, T.A.; Løvvik, O.M.; Aasmundtveit, K.E. A review of eutectic Au-Ge solder joints. *Metall. Mater. Trans. A* **2019**, *50*, 4632–4641. [[CrossRef](#)]
5. Rerek, T.; Skowronski, L.; Kobierski, M.; Naparty, M.K.; Derkowska-Zielinska, B. Microstructure and opto-electronic properties of Sn-rich Au-Sn diffusive solders. *Appl. Surf. Sci.* **2018**, *451*, 32–39. [[CrossRef](#)]
6. Živković, D.; Čubela, D.; Manasijević, D.; Balanović, L.; Gigović-Gekić, A.; Gomidželović, L.; Štrbac, N.; Mitovski, A. Thermal and structural characteristics of a eutectic Au-Ge alloy. *Mater. Test.* **2017**, *59*, 118–122. [[CrossRef](#)]
7. Kobayashia, T.; Ando, T. Recent development of joining and conductive materials for electronic components. *Mater. Trans.* **2021**, *62*, 1270–1276. [[CrossRef](#)]
8. Wang, X.; Zhang, L.; Li, M.L. Structure and properties of Au-Sn lead-free solders in electronic packaging. *Mater. Trans.* **2022**, *63*, 93–104. [[CrossRef](#)]
9. Larsson, A.; Aamundtveit, K.E. On the Microstructure of Off-Eutectic Au-Ge Joints: A High-Temperature Joint. *Metall. Mater. Trans. A* **2020**, *51*, 740–749. [[CrossRef](#)]
10. Wang, J.; Liu, H.S.; Liu, L.B.; Jin, Z.P. Thermodynamic description of Au-Ag-Si ternary system. *Trans. Nonferrous Met. Soc. China* **2007**, *17*, 1405–1411. [[CrossRef](#)]
11. Wang, J.; Liu, H.S.; Liu, L.B.; Jin, Z.P. Thermodynamic description of the Sn-Ag-Au ternary system. *Calphad* **2007**, *31*, 545–552. [[CrossRef](#)]
12. Wang, J.; Meng, F.G.; Rong, M.H.; Liu, L.B.; Jin, Z.P. Thermodynamic description of the Au-Ag-Pb ternary system. *Thermochim. Acta* **2010**, *505*, 79–85. [[CrossRef](#)]
13. Wang, J.; Meng, F.G.; Liu, H.S.; Liu, L.B.; Jin, Z.P. Thermodynamic modeling of the Au-Bi-Sb ternary system. *J. Electron. Mater.* **2007**, *36*, 568–577. [[CrossRef](#)]
14. Wang, J.; Leinenbach, C.; Roth, M. Thermodynamic modeling of the Au-Ge-Sn ternary system. *J. Alloys Compd.* **2009**, *481*, 830–836. [[CrossRef](#)]
15. Wang, J.; Leinenbach, C.; Roth, M. Thermodynamic description of the Au-Ge-Sb ternary system. *J. Alloys Compd.* **2009**, *485*, 577–582. [[CrossRef](#)]
16. Jin, S.; Duarte, L.I.; Leinenbach, C. Experimental study and thermodynamic description of the Au-Cu-Ge system. *J. Alloys Compd.* **2014**, *588*, 7–16. [[CrossRef](#)]
17. Jin, S.; Duarte, L.I.; Huang, G.; Leinenbach, C. Experimental investigation and thermodynamic modeling of the Au-Ge-Ni system. *Monatshefte Für Chem.-Chem. Mon.* **2012**, *143*, 1263–1274. [[CrossRef](#)]
18. Liu, H.S.; Liu, C.L.; Ishida, K.; Jin, Z.P. Thermodynamic modeling of the Au-In-Sn system. *J. Electron. Mater.* **2003**, *32*, 1290–1296. [[CrossRef](#)]
19. Wang, J.; Liu, Y.J.; Liu, L.B.; Zhou, H.Y.; Jin, Z.P. Thermodynamic modeling of the Au-Sb-Si ternary system. *J. Alloys Compd.* **2011**, *509*, 3057–3064. [[CrossRef](#)]

20. Meng, F.G.; Liu, H.S.; Liu, L.B.; Jin, Z.P. Thermodynamic description of the Au-Si-Sn system. *J. Alloys Compd.* **2007**, *431*, 292–297. [[CrossRef](#)]
21. Liu, J.; Guo, C.; Li, C.; Du, Z. Thermodynamic optimization of the Ge-Sb and Ge-Sb-Sn systems. *Thermochim. Acta* **2011**, *520*, 38–47. [[CrossRef](#)]
22. Okamoto, H.; Massalski, T.B. The Au-Ge (gold-germanium) system. *Bull. Alloy Phase Diagr.* **1984**, *5*, 601–610. [[CrossRef](#)]
23. Chevalier, P.Y. A thermodynamic evaluation of the Au-Ge and Au-Si systems. *Thermochim. Acta* **1989**, *141*, 217–226. [[CrossRef](#)]
24. Dinsdale, A.T. SGTE data for pure elements. *Calphad* **1991**, *15*, 317–425. [[CrossRef](#)]
25. Ansara, I.; Nabot, J.P. A thermodynamic assessment of the Au-In system. *Thermochim. Acta* **1988**, *129*, 89–97. [[CrossRef](#)]
26. Liu, H.S.; Cui, Y.; Ishida, K.; Jin, Z.P. Thermodynamic reassessment of the Au-In binary system. *Calphad* **2003**, *27*, 27–37. [[CrossRef](#)]
27. Chevalier, P.Y. A thermodynamic evaluation of the Ge-In, Ge-Pb, Ge-Sb, Ge-Tl and Ge-Zn systems. *Thermochim. Acta* **1989**, *155*, 227–240. [[CrossRef](#)]
28. Butt, M.T.Z. Study of Gold-Based Alloy Phase Diagrams. Ph.D. Thesis, Brunel University School of Engineering and Design, London, UK, 1990.
29. Chevalier, P.Y. A thermodynamic evaluation of the Au-Sb and Au-Tl systems. *Thermochim. Acta* **1989**, *155*, 211–225. [[CrossRef](#)]
30. Kim, J.H.; Jeong, S.W.; Lee, H.M. A thermodynamic study of phase equilibria in the Au-Sb-Sn solder system. *J. Electron. Mater.* **2002**, *31*, 557–563. [[CrossRef](#)]
31. Liu, H.S.; Liu, C.L.; Wang, C.; Jin, Z.P.; Ishida, K. Thermodynamic modeling of the Au-In-Sb ternary system. *J. Electron. Mater.* **2003**, *32*, 81–88. [[CrossRef](#)]
32. Gierlotka, W. Thermodynamic description of the binary Au-Sb and ternary Au-In-Sb systems. *J. Alloys Compd.* **2013**, *579*, 533–539. [[CrossRef](#)]
33. Zwingmann, G. Das Dreistoffsystem Gold-Antimon-Germanium. *Z. Fuer Met.* **1964**, *55*, 192–194. [[CrossRef](#)]
34. Prince, A.; Raynor, G.V.; Evans, D.S. *Phase Diagrams of Ternary Gold Alloys*; The Institute of Metals: London, UK, 1990; pp. 7–42.
35. Olesinski, R.W.; Abbaschian, G.J. The Ge-Si (germanium-silicon) system. *Bull. Alloy Phase Diagr.* **1984**, *5*, 180–183. [[CrossRef](#)]
36. Bergman, C.; Chastel, R.; Castanet, R. Thermodynamic investigation on the Si-Ge binary system by calorimetry and Knudsen cell mass spectrometry. *J. Phase Equilibria* **1992**, *13*, 113–118. [[CrossRef](#)]
37. Predel, B.; Bankstahl, H.; Gödecke, T. Die Zustandsdiagramme Silber-Germanium-Silizium und Gold-Germanium-Silizium. *J. Less-Common Met.* **1976**, *44*, 39–49. [[CrossRef](#)]
38. Okamoto, H.; Massalski, T.B. The Au-Sn (Gold-tin) system. *Bull. Alloy Phase Diagr.* **1984**, *5*, 492–503. [[CrossRef](#)]
39. Ipser, H.; Krachler, R. The AuZn melting diagram in the range of the β' -AuZn phase. *Scr. Metall.* **1988**, *22*, 1651–1654. [[CrossRef](#)]
40. Liu, H.S.; Ishida, K.; Jin, Z.P.; Du, Y. Thermodynamic assessment of the Au-Zn binary system. *Intermetallics* **2003**, *11*, 987–994. [[CrossRef](#)]
41. Butt, M.T.Z.; Bodsworth, C.; Prince, A. The AuZn-Ge section of the Au-Ge-Zn ternary system. *Scr. Metall.* **1989**, *23*, 1105–1107. [[CrossRef](#)]
42. Redlich, O.; Kister, A.T. Thermodynamics of nonelectrolyte solutions. *Ind. Eng. Chem.* **1948**, *40*, 341–345. [[CrossRef](#)]
43. Muggianu, M.Y.; Gambino, M.; Bros, J.P. Enthalpies of formation of liquid alloys bismuth-gallium-tin at 723K—choice of an analytical representation of integral and partial thermodynamic functions of mixing for this ternary-system. *J. Chim. Phys. Phys.-Chim. Biol.* **1975**, *72*, 83–88. [[CrossRef](#)]
44. Sundman, B.; Jansson, B.; Andersson, J.O. The thermo-calc databank system. *Calphad* **1985**, *9*, 153–190. [[CrossRef](#)]

Disclaimer/Publisher's Note: The statements, opinions and data contained in all publications are solely those of the individual author(s) and contributor(s) and not of MDPI and/or the editor(s). MDPI and/or the editor(s) disclaim responsibility for any injury to people or property resulting from any ideas, methods, instructions or products referred to in the content.